Chinese Journal of Aeronautics, (2019), 32(5): 1190–1203

Chinese Society of Aeronautics and Astronautics
& Beihang University

Chinese Journal of Aeronautics

cja@buaa.edu.cn
www.sciencedirect.com

Leading-edge flow separation control over an airfoil using a symmetrical dielectric barrier discharge plasma actuator

Xin ZHANG [a,*], Huaxing LI [a], Yong HUANG [b], Kun TANG [b], Wanbo WANG [b]

[a] School of Aeronautics, Northwestern Polytechnical University, Xi'an 710072, China
[b] Low Speed Aerodynamics Institute, China Aerodynamics Research and Development Center, Mianyang 621000, China

Received 21 March 2018; revised 22 May 2018; accepted 4 July 2018
Available online 21 March 2019

KEYWORDS

Airfoil;
Dielectric Barrier Discharge (DBD);
Flow control;
Particle Image Velocimetry (PIV);
Plasma actuator

Abstract In order to promote an in-depth understanding of the mechanism of leading-edge flow separation control over an airfoil using a symmetrical Dielectric Barrier Discharge (DBD) plasma actuator excited by a steady-mode excitation, an experimental investigation of an SC (2)-0714 supercritical airfoil with a symmetrical DBD plasma actuator was performed in a closed chamber and a low-speed wind tunnel. The plasma actuator was mounted at the leading edge of the airfoil. Time-resolved Particle Image Velocimetry (PIV) results of the near-wall region in quiescent air suggested that the symmetrical DBD plasma actuator could induce some coherent structures in the separated shear layer, and these structures were linked to a dominant frequency of f_0 = 39 Hz when the peak-to-peak voltage of the plasma actuator was 9.8 kV. In addition, an analysis of flow structures without and with plasma actuation around the upper side of the airfoil at an angle of attack of 18° for a wind speed of 3 m/s (Reynolds number Re = 20000) indicated that the dynamic process of leading-edge flow separation control over an airfoil could be divided into three stages. Initially, this plasma actuator could reinforce the shedding vortices in the separated shear layer. Then, these vortical structures could deflect the separated flow towards the wall by promoting the mixing between the outside flow with a high kinetic energy and the flow near the surface. After that, the plasma actuator induced a series of rolling vortices in the vicinity of the suction side of the airfoil, and these vortical structures could transfer momentum from the leading edge of the airfoil to the separated region, resulting in a reattachment of the separated flow around the airfoil.

1. Introduction

Flow separation usually causes some negative impacts on the aerodynamic performance of aircraft and land vehicles. Thus, investigations on flow separation control using passive flow control devices such as vortex generator,[1,2] gurney flap,[3,4]

* Corresponding author.
E-mail address: lookzx@mail.ustc.edu.cn (X. ZHANG).
Peer review under responsibility of Editorial Committee of CJA.

ELSEVIER Production and hosting by Elsevier

https://doi.org/10.1016/j.cja.2019.03.010

and active flow control devices, which includes blowing,[5] suction,[6] and synthetic jet,[7,8] have grabbed the attentions of many researchers. Compared to passive flow control actuators which only affect a flow at the pre-design status, an active flow control strategy is more flexible and thriving.

Flow control using a Dielectric Barrier Discharge (DBD) plasma actuator is one of the active flow control methods. DBD plasma actuators have been extensively investigated over the past two decades[9–18] and demonstrated to be a novel method for broadband noise control,[19–21] lift augmentation,[22–25] transition control,[26–28] and cylinder wakes control,[29,30] thanks to its significant properties, such as no moving parts, fast response, and a control capacity of wide band.

A traditional DBD plasma actuator includes two electrodes which are separated by a thin insulating film.[31–37] One electrode is exposed to the air, and the other is covered by a dielectric film, as shown in Fig. 1. When the electrodes are excited by an AC high-voltage power at several kHz, the air around the exposed electrode is ionized rapidly, and non-thermal plasma is generated.

Since flow separation control using a DBD plasma actuator is an effective method to enhance the aerodynamic performances of airfoils, a number of researchers have been involved in this study field using wind tunnel experiments and numerical simulation over the last decade.[38–45] A pioneering investigation of flow separation control by a DBD plasma actuator over an airfoil was conducted by Post and Corke,[46] who demonstrated that the separated flow around an airfoil at a high angle of attack could be suppressed by a plasma actuator which was arranged at the leading edge of the airfoil. Then, in order to enhance the control effect of flow separation control using a DBD plasma actuator, some key parameters, such as actuation position,[47] voltage amplitude,[40] actuator geometry,[48] and actuation strategies (steady and unsteady operations),[49] have been investigated by lots of researchers.

However, most of the investigations evaluated the ability of a DBD plasma actuator for flow separation control by force measurements, mean pressure distribution, and time-averaged velocity fields around the upper side surface of an airfoil. The controlling mechanisms of the interaction between the induced airflow by a plasma actuator and the separated flow have not been completely elucidated.

To clarify the mechanism of flow separation control, Benard and Moreau carried out wind tunnel experiments to study the process of separation flow control using Particle Image Velocimetry (PIV) technology.[50] In this study, an asymmetrical DBD plasma actuator driven by a steady operation was placed at the leading edge of a NACA 0015 airfoil at a Reynolds number of 260000. They found that the plasma actuator could reinforce the flow structures that already existed in the based flow, leading to a mixing between the mean airflow and the boundary layer. These investigations have enhanced our understanding of the mechanism of flow separation using a plasma actuator. However, due to the limited spatial resolution of the PIV device, the flow structures which were close to the wall couldn't be obtained. Greenblatt et al. focused on the mechanism of separated flow control over a flat plate airfoil under unsteady DBD plasma actuation at a Reynolds number of 3000 by wind tunnel experiments and computational investigation.[51] They suggested that the most effective pulsed frequency for lift enhancement was in connection with the frequency of vortex shedding of the bluff body, and the key point of flow separation control was to excite the leading edge vortical layer. Meanwhile, Sato et al. studied the mechanism of flow separation control over a NACA 0015 airfoil with unsteady operation at a low Reynolds number using large eddy simulation.[49] They found that the unsteady DBD plasma actuator driven by a higher non-dimensionalized pulsed frequency F^+ could induce a train of turbulent vortices and more effectively suppress the laminar separated flow. Recently, Sekimoto et al. carried out wind tunnel experiments to figure out the relationship between the induced vortex structure and the pulsed frequency of a DBD plasma actuator using time-averaged pressure measurement and PIV technology.[52] They suggested that the size of the induced vortex was increased with a decreasing pulsed frequency of the plasma actuator. However, this investigation just showed the time-averaged flow field and did not describe the evolution process of the induced vortex.

In general, these previous research efforts[49–52] help us understand the mechanisms of flow separation control using steady and unsteady plasma actuation. Although a number of researchers prefer to use the unsteady excitation of a plasma actuator which is switched on and off with a variable cycle for saving energy consumption and improving the control effect, a consensus about the optimal non-dimensionalized pulsed frequency of a plasma actuator has not been reached yet.[52] Meanwhile, there was almost no difference between steady and unsteady actuation at Mach 0.35 and 0.4 based on increments of the averaged lift, which was proven by Kelley et al.[40]

Despite the previous investigations towards describing the dynamic process of flow separation control by unsteady plasma actuation, insight into the flow structures in the vicinity of airfoil surface, as well as the interaction between the induced airflow by a plasma actuator and the separated flow, remains limited. Meanwhile, in view of the remarkable differences between steady and unsteady excitation, these previous results about unsteady control mechanisms[49,52] cannot completely represent the controlling mechanism of steady actuation of a symmetrical plasma actuator.

The main aim of the present investigation is to study the process of formation, development, and evolution of some coherent structures induced by a symmetrical plasma actuator in quiescent air and their functions in flow separation control with incoming flow. Here, a symmetrical DBD plasma actuator driven by a steady operation is placed at the leading edge of an SC (2)-0714 supercritical airfoil. In the following sections, the experimental setup is discussed first. Then, a time-resolved PIV system is adopted to measure the airflow field

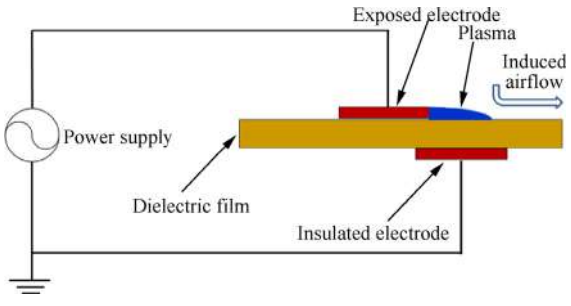

Fig. 1 Schematic diagram of a typical DBD plasma actuator.

induced by the plasma actuator without incoming flow. Moreover, the third section focuses on a detailed study of flow structures around the airfoil without and with a symmetrical plasma actuator to fully describe the interaction between the induced flow by the plasma actuator and the separated flow for deepening the understanding on the controlling mechanism of the symmetrical plasma actuator.

2. Experimental set-up

2.1. Experiments in quiescent air

A high-speed PIV system supported by LAVISION Company was used to investigate the transient flow field induced by a plasma actuator. Fig. 2 presents the equipment layout of PIV experiments in quiescent air. An SC (2)-0714 supercritical airfoil model with a DBD plasma actuator was placed in a cubic chamber with a size of 600 mm (width) × 600 mm (height) × 800 mm (length) to make sure that the flow field induced by the plasma actuator was not influenced by the environment. PIV laser was mounted on the top of the chamber, and a high-speed CCD camera which had a spatial resolution of 1024 pixel × 1024 pixel was arranged on the side of the chamber and used to view a region of 18 mm × 18 mm. Image pairs were recorded at a frequency of 3 kHz with the time delay between frames in a pair being usually 200 μs. The sampling duration was 6 s. The DEHS (Di-Ethyl-Hexyl-Sebacate) particles which were used to seed the air through the input of the chamber were about 1 μm in diameter and produced by an LASKIN-40 smoker. The velocity and vorticity fields of the induced airflow were calculated by LAVISION PIV software, using a cross-correlation algorithm and a local median filter to produce vectors over a 16 pixel × 16 pixel interrogation window with 50% overlap for obtaining an accuracy of 3%–5%. Five small holes located in the lower left corner of the chamber were used for cable running.

A symmetrical plasma actuator which had the ability to control the flow separation around an airfoil at a high wind speed and a high Reynolds number comparing to a traditional asymmetrical plasma actuator[53,54] was adopted and actuated by a steady operation in this study. The main layout difference between an asymmetrical plasma actuator and a symmetrical one is the lower electrode, as shown in Fig. 3. The lower electrode of the symmetrical plasma actuator covers the whole upper electrode, and thus this actuator could generate bi-directional plasma on both sides of the upper electrode. The plasma actuator was actuated by an AC power supply. The range of working frequency is from 0.1 to 6 kHz, and the voltage amplitude ranged from 0 to 10 kV. The output waveform for an amplitude of 8 kV and a frequency of 1 kHz was obtained by a Tektronix oscilloscope, as shown in Fig. 4.

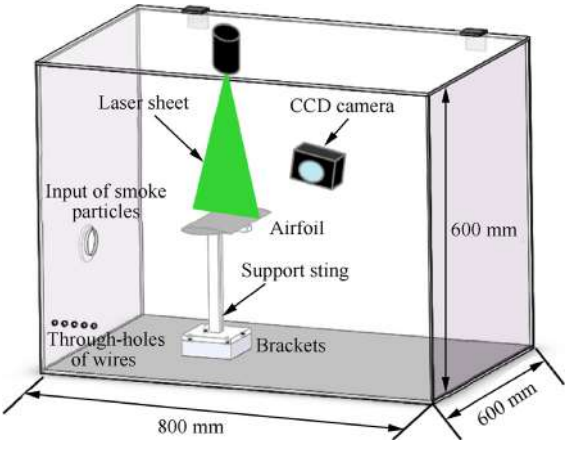

Fig. 2 Schematic diagram of experimental set-up.

The testing model was a two-dimensional SC (2)-0714 supercritical wing which had a 25° swept leading edge with a chord length of 100 mm and a spanwise length of 480 mm, as presented in Fig. 5. Fig. 6 shows a schematic diagram of the airfoil and a symmetrical plasma actuator. The exposed electrode which was mounted on the suction side of the airfoil near the leading edge was copper foil tape. It was 2 mm wide and 0.02 mm thick. The covered electrode was the whole testing model which was made of aluminum. The upper electrode was attached to the high-voltage power which provided a few kilovolts of AC voltage power, whereas the lower electrode was attached to the ground. The insulating material was two layers of Kapton film, and the thickness of each layer was 0.05 mm. The origin of the coordinate system was fixed at the midpoint of the exposed electrode. The x-axis paralleled to the streamwise flow, and the y-axis pointed to the vertical direction.

2.2. Experiments in a low-speed wind tunnel

Experimental investigations were carried out at the China Aerodynamics Research and Development Center (CARDC) in an open-section low-speed wind tunnel with a size of 750 mm (width) × 750 mm (height) × 1050 mm (length). The main parts of the wind tunnel are made of dielectric material fiberglass, which is suitable for research on plasma flow control. A Pitot tube was adopted to monitor the incoming flow velocity at the entrance of the test section. The wind velocity range was 2–55 m/s and the turbulence intensity was less than 0.2%.

An airfoil with a DBD plasma actuator in this study is the same as that in the experiment of characterization of a plasma actuator in still air, as shown in Fig. 5. Fig. 7 shows the supercritical airfoil mounted in the test section. The testing model was held vertically between two plates which were applied to generate a two-dimensional flow around the airfoil. The upper plate was constructed from 10 mm-thick clear Plexiglas which was suitable for flow visualization experiments. A support

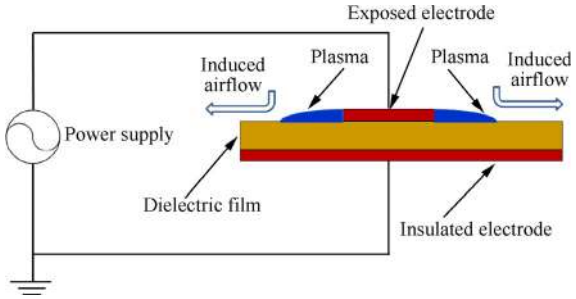

Fig. 3 Electrode configuration of a symmetrical DBD plasma actuator.

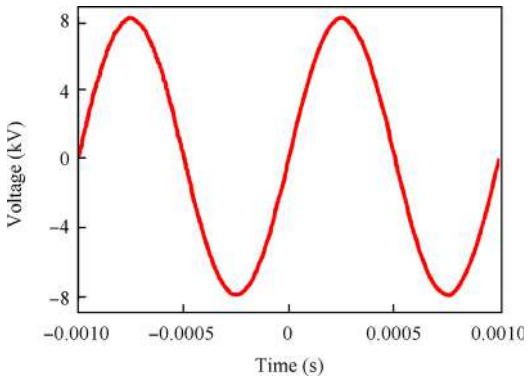

Fig. 4 Plasma discharge voltage waveform.

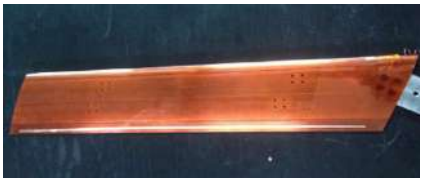

Fig. 5 Image of supercritical airfoil.

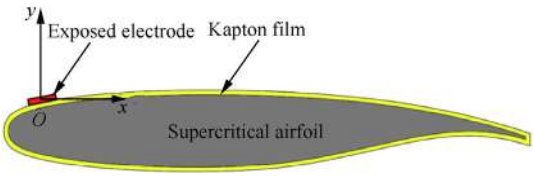

Fig. 6 Schematic diagram of electrode configuration of symmetrical plasma actuator.

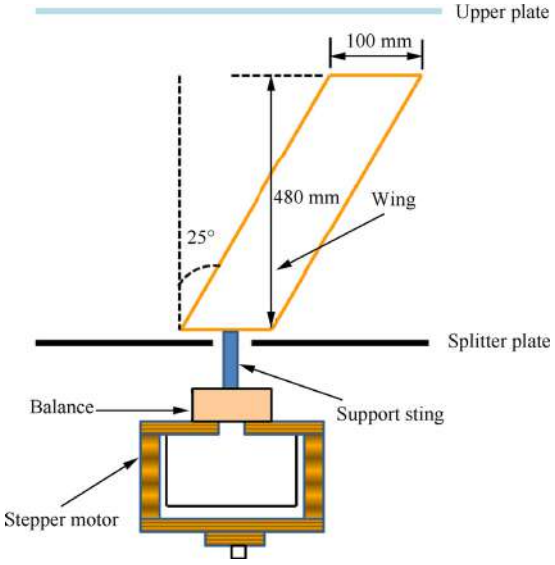

Fig. 7 Schematic diagram of supercritical airfoil in a low-speed wind tunnel.

sting supported the testing model through a hole at the quarter chord location in the lower panel. The model was connected to a force balance by way of the support sting. The angular position of the airfoil model was controlled by a stepper motor on the balance. The maximum error of the angle of attack of the airfoil was $\pm 0.05°$. The incoming flow speed was set to 3 m/s, and the Reynolds number which was based on the chord length of the airfoil was 20000.

The PIV system is the same as that used in the chamber experiments without incoming flow. The layout of the PIV device is shown in Fig. 8. A CCD camera was mounted above the ceiling plane. The laser sheet was perpendicular to the upper side of the airfoil and intersected with the airfoil at the mid-span location. The angle between the CCD camera and the laser sheet was 90°. In order to improve the spatial resolution, the view of the flow field focused on the leading edge of the airfoil. The size of the window was just 32 mm × 32 mm.

3. Results and discussion

Discussion of results is divided into three parts. The first section studies the characteristics of a symmetrical DBD plasma actuator in still air. Then, the second part focuses on an in-depth investigation of the based flow to reveal the dynamic process of the vortical structures which are shedding from the leading edge of the airfoil. The third part aims to compare the flow fields without and with plasma actuation and analyze the mechanism of flow separation control using a steady plasma excitation.

3.1. Characterization of a symmetrical DBD plasma actuator in quiescent air

3.1.1. Time-averaged flow field

Fig. 9 shows time-averaged velocity fields above the upper electrode in quiescent air with two different peak-to-peak voltage amplitudes $U_{p\text{-}p}$. Here, U_p and V_p are flow speed induced by plasma actuator in the x and y directions, respectively, $x^* = x/c$ is the non-dimensional distance in the horizontal direction, $y^* = y/c$ is the non-dimensional distance in the normal direction, c is the mean aerodynamic chord length of the airfoil, and f is the actuation frequency of high-voltage power supply. The ambient air is deflected towards the surface of the airfoil, and then ejected from the exposed electrode. The induced airflow is similar to a traditional wall jet, but there is no mass added to the airflow.[11,12] Due to the symmetry,

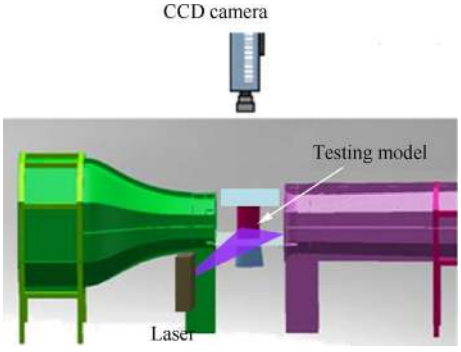

Fig. 8 Schematic diagram of experimental set-up for PIV experiments in a low-speed wind tunnel.

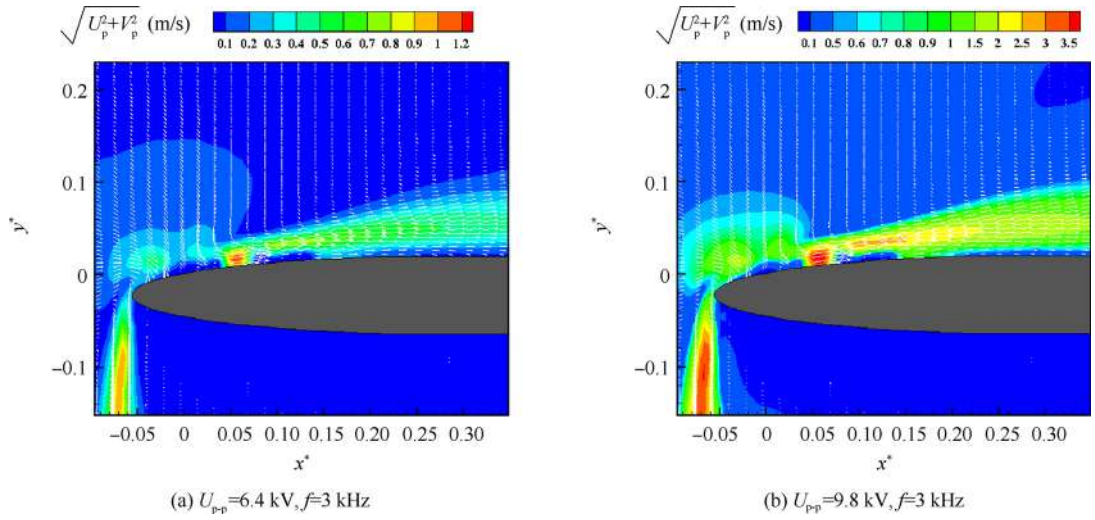

Fig. 9 Time-averaged velocity fields above actuator in quiescent air.

the actuator induces a bi-directional wall jet on each side of the upper electrode. The maximum velocities of two jets induced by a plasma actuator are approximately equal. In addition, the maximum velocity of a plasma jet increases with the voltage amplitude.

3.1.2. Spatial and temporal characteristics

Fig. 10 is a snapshot of the flow field induced by a plasma actuator in quiescent air. Since the plasma actuator is activated, the mutual effect between the plasma and the surrounding air leads to a starting vortex which is located above the exposed electrode. There are no coherent structures which are close to the wall when the peak-to-peak voltage amplitude is 6.4 kV, as presented in Fig. 10(a). However, as the voltage amplitude is increased, the induced airflow has some coherent structures, such as roll-up vortices and secondary vortices, which are close to the airfoil upper surface, as shown in Fig. 10(b). The shear layer of the plasma wall jet becomes unstable with increasing the voltage amplitude. The induced airflow generates a roll-up vortex in the shear layer of the plasma wall jet. As time goes on, the roll-up vortices stretch and move along the airfoil upper surface and form a train of vortices. Meanwhile, due to the no-slip boundary condition, secondary vortices are formed over the airfoil upper surface. The secondary vortices are underneath the roll-up vortices and move along the airfoil surface.

It is worth noting that there are some differences between roll-up vortices and the starting vortex. Initially, the formation mechanism is different. When the plasma actuator reaches the threshold voltage, the air near the upper electrode could be ionized and carry the momentum to the flow field. To replenish the flow that has been ejected, entrainment occurs above the upper electrode to generate a starting vortex. However, roll-up vortices could be generated due to the instability of the shear layer. In addition, the size of the starting vortex is bigger than those of roll-up vortices. Meanwhile, the trajectory is different between the starting vortex and the roll-up vortices. The starting vortex could roll up and move away from the wall. The moving trajectory of roll-up vortices, however, is near the wall. Moreover, the starting vortex is a single vortical structure, while roll-up vortices are a train of vortices. The roll-up vortices have the process of formation, movement, merging, and breakdown.

3.1.3. Coherent structures

From the discussion above, the results suggest that the types of plasma jet are related to the voltage amplitude. When the voltage amplitude is higher, the plasma jet could be a turbulent jet

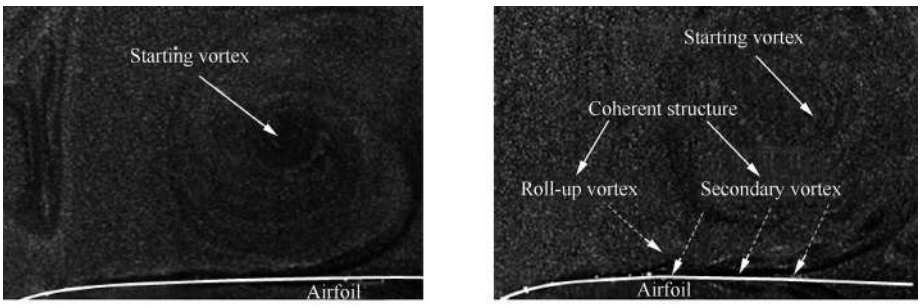

Fig.10 Original PIV images of flow field induced by a plasma actuator in quiescent air (t = 0.85 s).

which includes coherent structures near the wall. These could promote the mixing effect of the plasma actuator which is beneficial for separation flow control at a high wind speed and a high Reynolds number. Therefore, the coherent structures induced by the plasma actuator will be analyzed in this section.

According to the transient flow field results, the roll-up and secondary vortices move to the trailing edge of the airfoil. Although the induced flow field is unsteady, it still has quasi-periodic characteristics, as indicated by the power spectrum of velocity data in the shear layer over the surface. The positions of calculation points A to C are shown in Fig. 11. In order to get a precise comparison of the power spectrum, the calculation points are collected at a y position which corresponds to the maximum Root Mean Square (RMS) velocity.

Fig. 12 shows power spectra of the vertical fluctuating velocity at different places of the airfoil. At Point A, a dominant frequency of $f_0 = 39$ Hz is amplified in the shear layer when the plasma actuator is excited by a higher voltage, as shown in Fig. 12(a). The instability of the shear layer could force a vortex to roll up in the shear layer. Then disturbances start to grow, and a sub harmonic of the dominant frequency of 22 Hz is emerged at Point B, as shown in Fig. 12(b). It is suggested that roll-up vortices could be merged, and the interactions between the disturbances are nonlinear.[55] However, it is worth noting that the velocity spectrum in Fig. 12(b) displays a peak at 22 Hz which is somewhat less pronounced than a fundamental peak at 39 Hz, which indicates that the merging of the roll-up vortices in the separated shear layer could not be very notable. Further downstream, there is no distinct peak in the power spectrum, as depicted in Fig. 12(c). It indicates that the roll-up vortices are rapidly broken down during the transition process.

According to the fundamental frequency f_0 of 39 Hz, one period was obtained. Fig. 13 shows an evolutionary process of the coherent structures in one cycle. Here, Λ_{ci} is defined by $\Lambda_{ci} \equiv \lambda_{ci} \frac{\omega}{|\omega|}$, where λ_{ci} is the imaginary part of the complex eigenvalue of the velocity gradient tensor,[56] which can represent the vortical structure, and ω is the vorticity. The sign of local vorticity is assigned to λ_{ci} for identifying the sense of rotation.[57]

Based on the swirling strength in these pictures, we can see that there are several vortices in the flow field. Firstly, the two single roll-up vortical structures which are marked as No. 1 and No. 2 are generated in the separated shear layer, as shown in Fig. 13(a). The two roll-up vortices move together downstream, as presented in Fig. 13(b)–(d). Furthermore, the spacing between the two roll-up vortices is approximately constant in these images, suggesting that they roll up at a constant frequency. Then another roll-up vortex which is labeled as No. 3 is induced, as shown in Fig. 13(e). As time goes by, a breakdown of vortex No. 1 occurs downstream of the airfoil, as depicted in Fig. 13(h). After that, the two vortices, namely No. 2 and No. 3, move to the trailing edge of the airfoil, which indicates that the roll-up vortexes have experienced one period, as shown in Fig. 13(i).

In addition, the roll-up vortices on the left side of the exposed electrode are also analyzed in this part. The location of calculation Point D is at $x = -2.7$ mm and $y = -4.6$ mm, which is depicted in Fig. 11.

Fig. 14 shows the power spectrum of the vertical fluctuating velocity at Point D. It is noteworthy that there is a primary frequency of $f_0 = 39$ Hz when the plasma actuator is driven by a higher voltage. The results indicates that the fundamental frequencies f_0 of roll-up vortices on both sides of the exposed electrode are equal. It implies that the fundamental frequency is related to the electric parameters, such as the frequency of the power supply, but is barely relevant to the location of the plasma actuator.

3.2. Based flow

3.2.1. Time-averaged flow field

Fig. 15 shows the time-averaged flow field around the upper side of the airfoil at an angle of attack of 18° without control. Here, U and V are the incoming flow speed components in the x and y directions, respectively, U_0 is the mean flow speed ($U_0 = 3$ m/s), λ_i is the imaginary part of the complex eigenvalue of the velocity gradient tensor, and TKE denotes turbulent kinetic energy. The baseline flow is dramatically separated close to the leading edge, which generates a remarkable low-speed flow region above the surface, as shown in Fig. 15(a). The time-averaged velocity field shown in Fig. 15(a) indicates that boundary layer separation starts at about $x/c = 0.06$ and $y/c = 0.015$ that is related to 1.5% of the mean chord length. Due to the flow separation, the vortices shed from the suction side of the airfoil, as presented in Fig. 15(b). Meanwhile, the time-averaged TKE, which is defined as $\text{TKE} = 0.5\sqrt{U'^2 + V'^2}/U_0$, is shown in Fig. 15(c). Here, U' and V' are the fluctuating velocity components in the x and y directions, respectively. The results indicates that the high-energy region increases rapidly in the separated shear layer after the flow is separated, suggesting that transition occurs and the flow becomes turbulent.

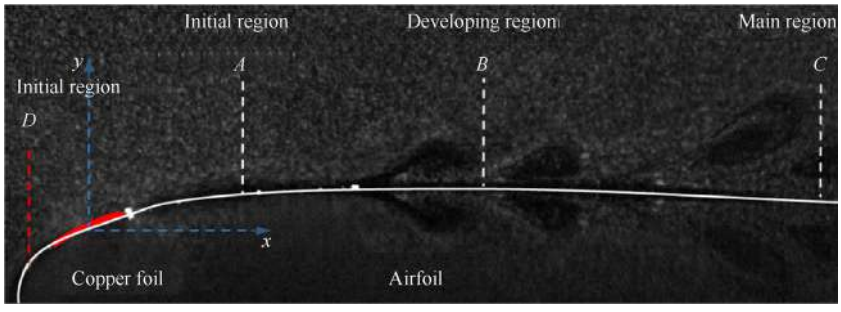

Fig. 11 Locations of calculation points A to C on right side of exposed electrode ($x_A = 3.2$ mm, $x_B = 6.5$ mm, $x_C = 13.3$ mm).

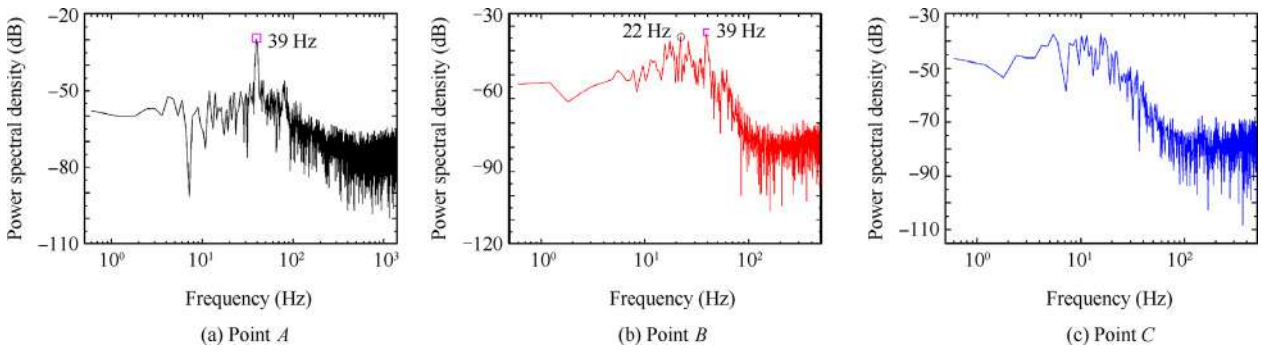

Fig. 12 Power spectra of vertical fluctuating velocity at different locations of right side of exposed electrode.

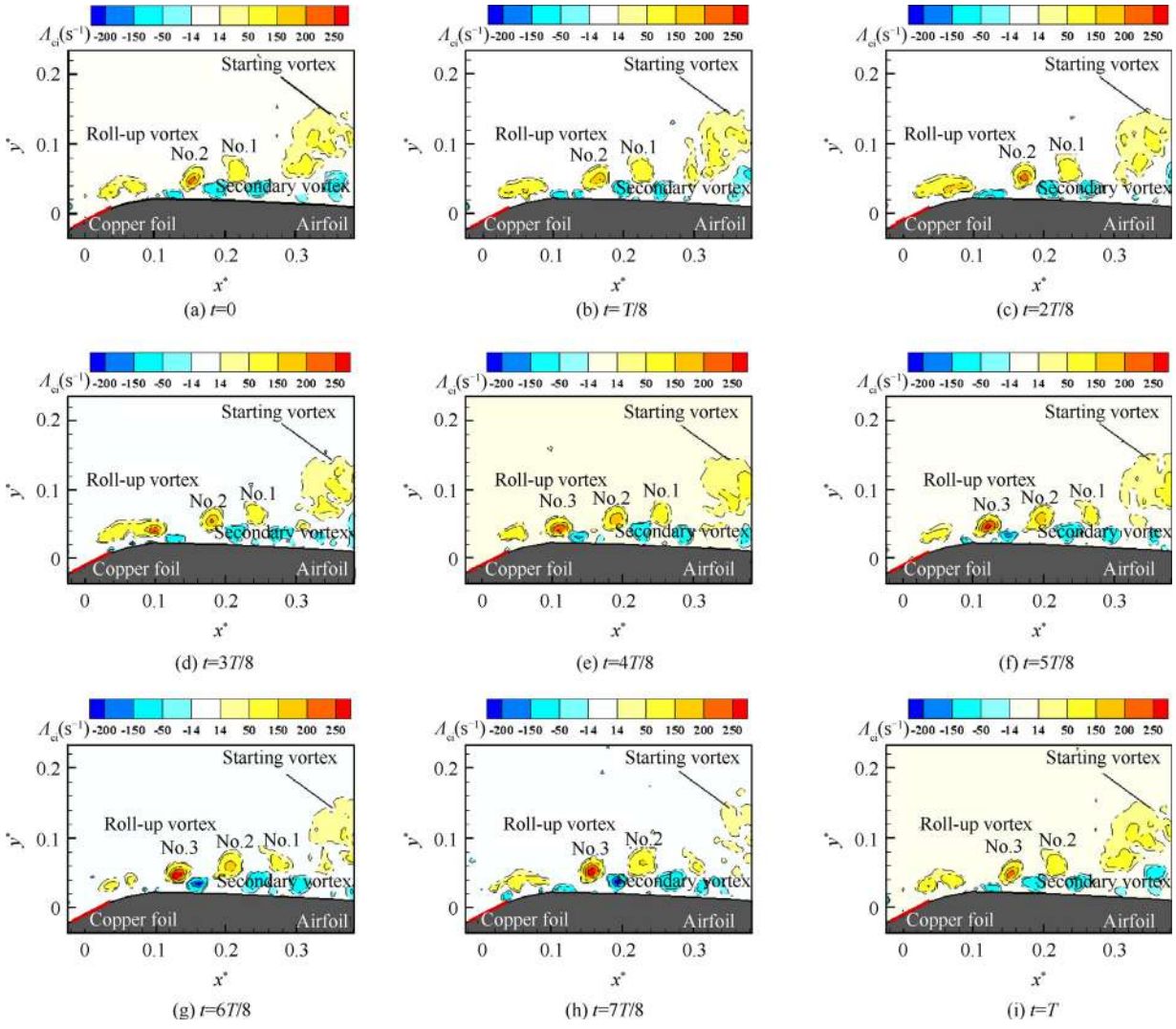

Fig. 13 Evolution of swirling strength field on right side of exposed electrode in one cycle (T stands for cycle time).

3.2.2. Dynamics of based flow field

In this part, analyses focus on vortex shedding from the separated shear layer using the swirling strength. Fig. 16 shows the dynamic process of the evolution of vortices which is issuing from the separated flow. Here, t_{off} means that the plasma actuator is turned off. Due to the flow separation, a series of small-scale vortices forms and grows along the separated shear layer, indicating that the flow remains completely separated along the upper surface of the airfoil. Meanwhile, the vortical structures that are shedding from the leading edge to the trailing edge can be distinguished by the swirling strength, suggesting a two-dimensional flow in this study. It should be noted that

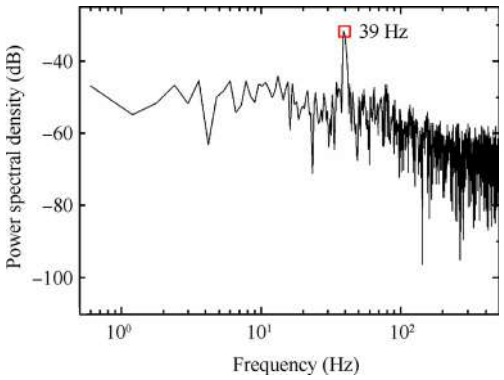

Fig. 14 Power spectrum of vertical fluctuating velocity in initial region of left side of exposed electrode.

these vortices form at roughly 1% of the mean chord length, but shed at approximately 3% of the averaged chord length. These vortices are convected and transfer the momentum from the outside region toward the surface of the airfoil. Unfortunately, these vortices are not strong enough to suppress the separation by mixing.[50]

In order to obtain the fundamental frequency of the shedding vortices, the spectra of the fluctuating velocity data on the upper side of the airfoil are analyzed, as depicted in Fig. 17. The calculation points are collected at a y position that corresponds to the maximum RMS velocity for getting an accurate comparison of the power spectrum. It is worth noting that there is a dominant frequency in the initial region, suggesting that the vortices in the separated shear layer roll up at the dominant frequency which is related to flow disturbances,[55] as presented in Fig. 17(a). This result agrees with those of previous investigations that the dominant frequency reveals a power-law dependency on the Reynolds number.[58] In addition, these periodic flow disturbances could induce the separated shear layer to roll up and generate these vortical structures. This dynamic process is similar to the condition of free shear layers and consistent with previous results by Lang et al.[59] Then the flow shown in Fig. 17(b)–(d) experiences a rapid laminar-to-turbulent transition, with a typical spectrum found at $x^* = 0.1$–0.3.

3.3. Flow controlled by a symmetrical DBD plasma actuator

In the previous section, the results have indicated that a plasma actuator which is excited by a higher voltage can generate a turbulent jet. This part will focus on the controlled flow by a plasma actuator which can induce a turbulent jet around the airfoil and is described using time-averaged and time-resolved PIV results.

3.3.1. Time-averaged flow field

The time-averaged PIV results confirm the significant changes of flow around the upper side of the airfoil because of plasma actuation. The based flow is separated at the leading edge of the airfoil. With plasma actuation, flow separation is drastically reduced, and the controlled flow almost attaches to the airfoil surface, which can be proven by the time-averaged velocity field, as shown in Fig. 18(a). It should be noted that the flow is not fully attached to the surface of the airfoil with the plasma actuator. The maximum thickness of the separated flow is approximately 1 mm. This result agrees well with Roth's experimental result.[60] In order to get more detailed flow structures which are close to the wall, the field of PIV view is just 32 mm × 32 mm. Meanwhile, the airfoil model is painted with matt black lacquer for minimizing wall reflections. Thanks to the spatial resolution of PIV results, the detailed flow near the wall can be obtained. The discrete rolling vortices which are induced by the interaction between the plasma jet and the incoming flow and transfer momentum to the separated region are convected along the suction side of the airfoil, as shown in Fig. 18(b). It should be noted that the height of vortical structures is approximately equal to the thickness of the separated flow in the controlled flow field. The observation of a reattachment phenomenon controlled by an AC plasma actuator is not new.[53,54] However, the flow structures near the surface of the airfoil are rarely described. These results open new insight for understanding the controlling mechanism of a plasma actuator driven by an AC power.

In addition, the change induced by a plasma actuator to the flow field also produces modifications of the turbulent kinetic energy, as presented in Fig. 18(c). With plasma actuation, the flow near the upper surface of the airfoil has a higher turbulent kinetic energy than that of the based flow due to these discrete vortices, suggesting that the flow has stronger ability to resist an adverse pressure gradient and suppress flow separation.

Fig. 19 shows velocity profiles at different locations of the upper side of the airfoil. Here, y_s stands for the vertical distance from the upper surface of the airfoil. Without control, a negative velocity appears in the velocity profiles from $x^* = 0.1$ to 0.3, indicating that the flow is already separated. Thanks to the momentum induced by the plasma actuator, the velocity near the surface of the airfoil is increased, and

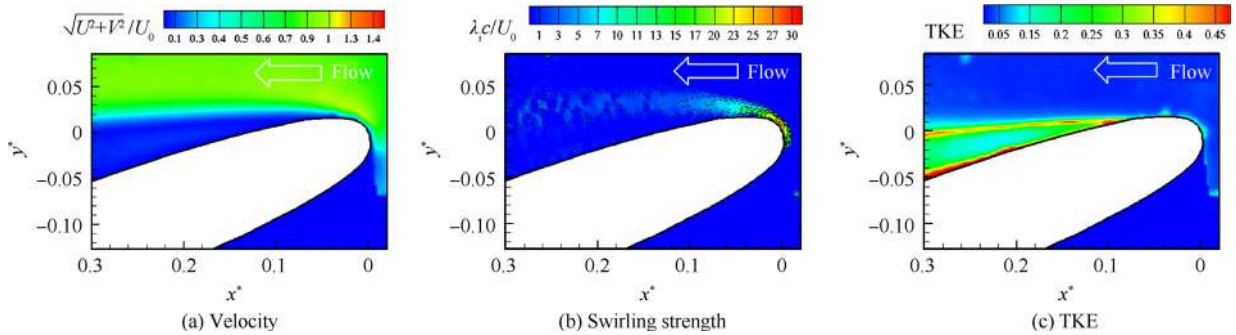

Fig. 15 Time-averaged PIV results without control.

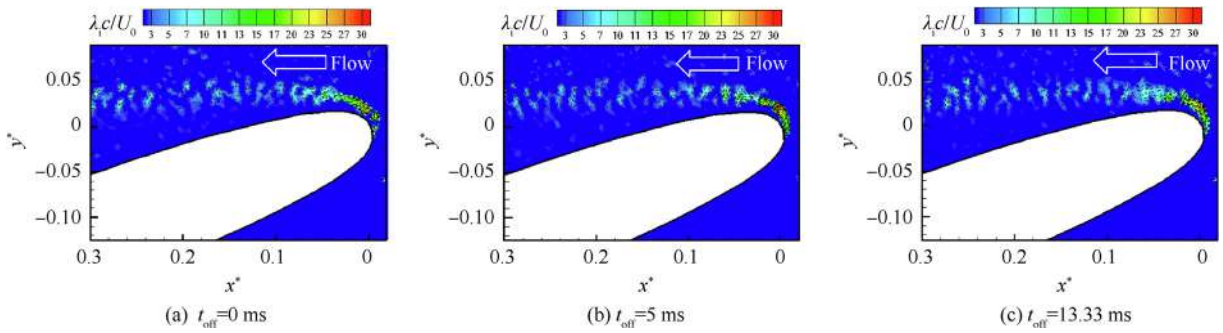

Fig. 16 Evolution of swirling strength field around upper side of airfoil without plasma actuation.

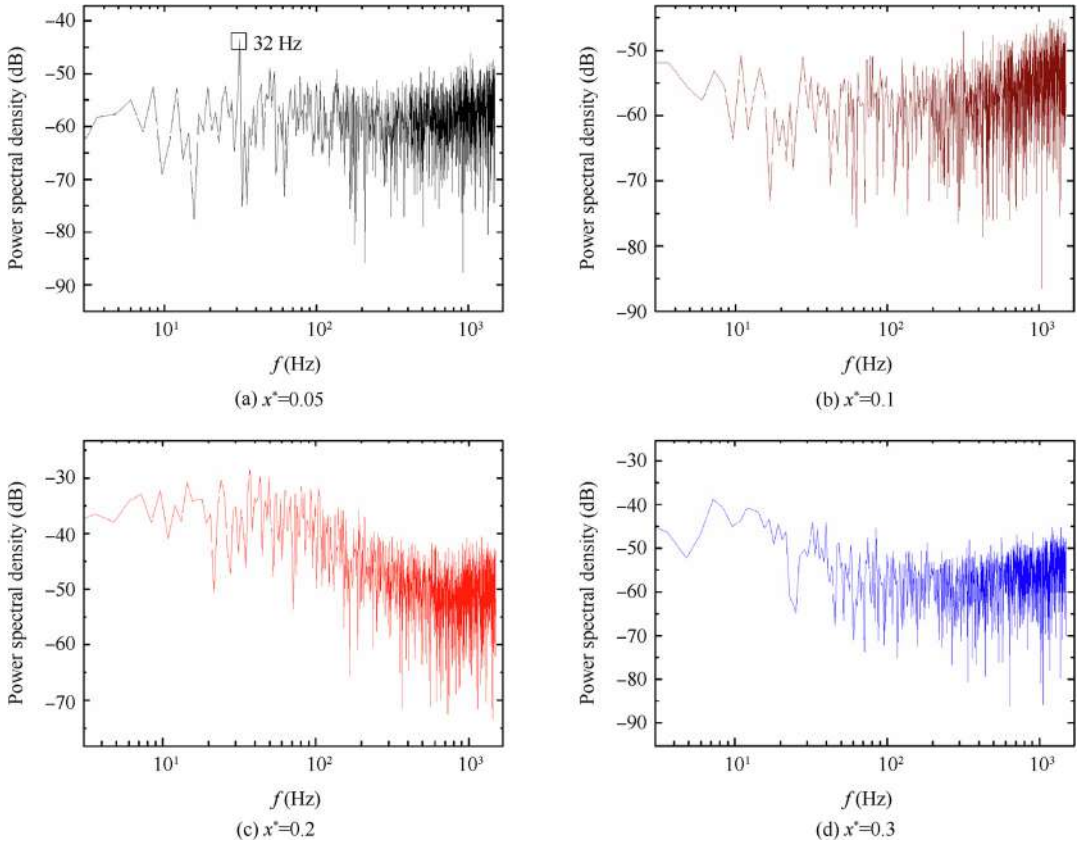

Fig. 17 Power spectra of vertical fluctuating velocity at different locations of upper side of airfoil without control.

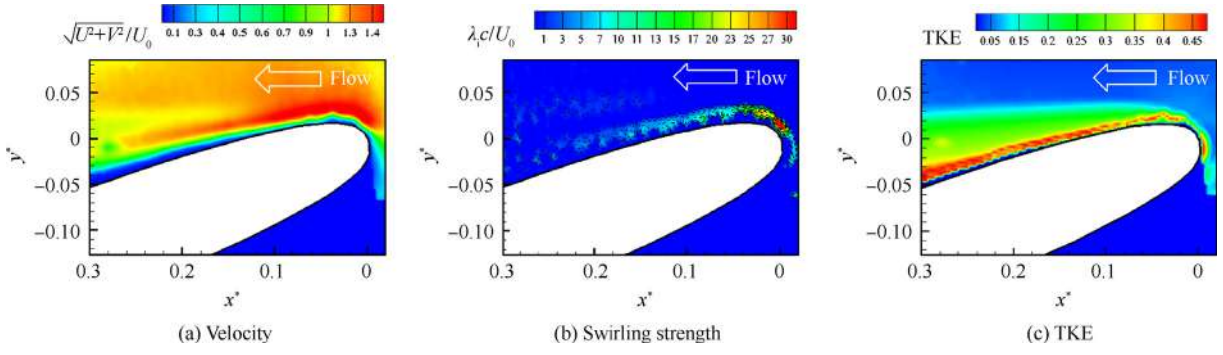

Fig. 18 Time-averaged PIV results around suction side of airfoil with a plasma actuator.

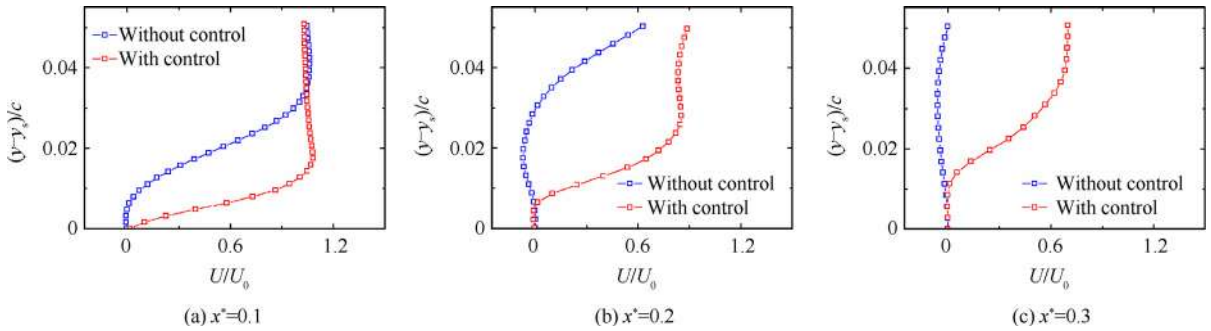

Fig. 19 Time-averaged velocity profiles along the suction side of airfoil without and with a plasma actuator.

the boundary layer becomes more energetic with plasma control. These results agree with those of previous investigations that obviously support a sufficient control effect of DBD plasma actuation to suppress flow separation and delay the stall angle of attack at the present Reynolds number.[58] In addition, the velocity profile is also affected by the plasma actuator at $x^* = 0.3$, which means that the plasma actuator could influence the flow field away from the leading edge of the airfoil through a convection of a series of small rolling vortices.

3.3.2. Dynamics of controlled flow field by plasma actuator

In this section, the controlling mechanism of the plasma actuator needs an in-depth investigation using time-resolved PIV measurements. Initially, instantaneous PIV results with the plasma actuator shown in Fig. 20 are analyzed for getting the reattachment processes of the flow around the suction side of the airfoil. Here, t_{on} means that the plasma actuator is switched on. The plasma actuator starts at t_{on} = 0 ms, and the plasma actuation lasts about 2 s.

At the beginning, a number of vortices are continuously rolling up and shedding from the separated shear layer towards the main flow, as depicted in Fig. 20(a). Then more energetic vortices are produced by the plasma actuator at the leading edge of the airfoil and involved in the separated region, which can be confirmed by the swirling strength, as shown in Fig. 20(b). After that, the separated flow is shifted downwards, and the separation region becomes smaller, as presented in Fig. 20(c). The interaction between the induced flow by the plasma actuator and the incoming flow plays an important role in controlling flow separation and enhancing the energy of rolling-up vortices in the separated shear layer, which bring more energy from the mainstream into the near-surface region. As time goes on, a series of vortical structures is convected along the upper side of the airfoil and contribute to the momentum transfer, as shown in Fig. 20(d)–(f). These results could reveal why the plasma actuator which is mounted at the leading edge of the airfoil can affect the flow structures at the trailing edge of the airfoil.

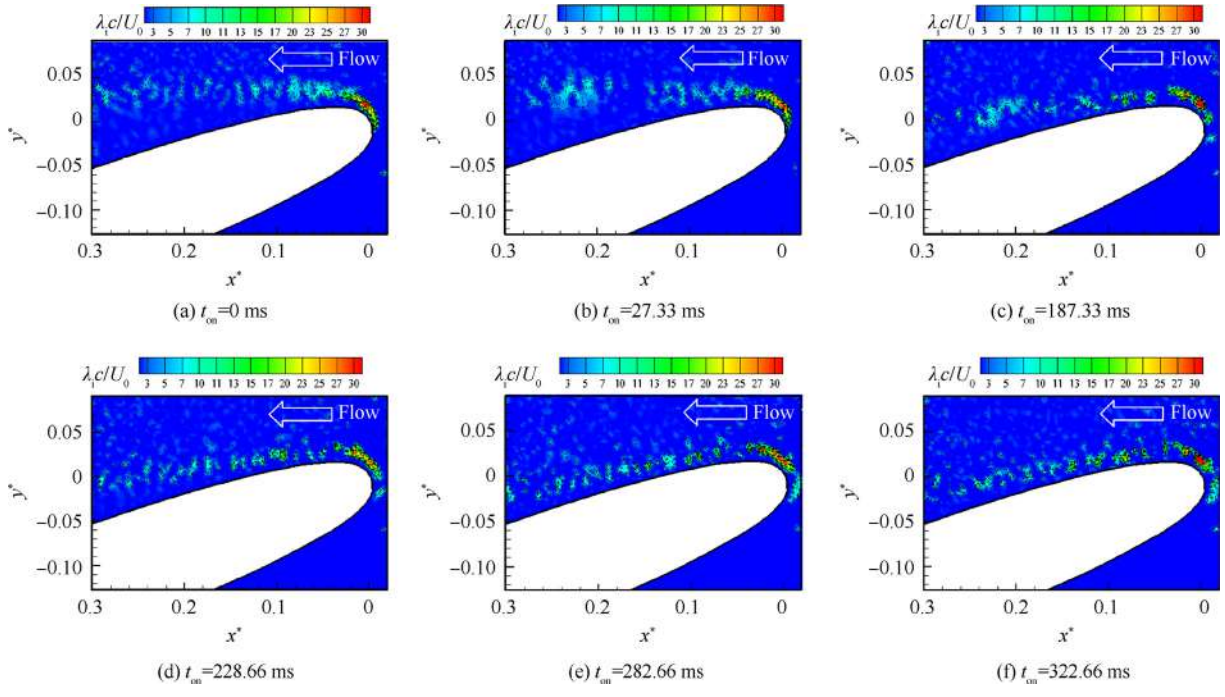

Fig. 20 Instantaneous swirling strength field around the upper side of airfoil with plasma actuation.

It is noteworthy that the controlled flow has reached a constant state at t_{on} = 282.66 ms, as shown in Fig. 20(e). In addition, the non-dimensional times t^+ which are required to suppress flow separation are approximately 12. Here, t^+ is defined by $t^+ = (t_0U_0)/(0.7c)$, where t_0 which is equal to 282.66 ms is the typical time needed to help the separated flow reattachment. 0.7 means the length of flow reattachment controlled by the plasma actuator. According to a previous investigation, the flow reattachment reached 70% of the chord length under a symmetrical plasma actuator. The time-scale of approximate 12 for the flow reattachment around an airfoil is similar to that found in investigations by Benard and Moreau.[50]

In general, observations of the controlling process can be divided into three stages. Firstly, the strength of shedding vortices in the separated shear layer is promoted, which can be confirmed by the swirling strength at the leading edge of the airfoil. The plasma actuator could play the role of a catalyzer in the first stage. Then, the separated flow is deflected towards the wall, and the separated region gradually becomes smaller due to the shedding vortices. Finally, quite a number of discrete rolling vortices which are generated by the interaction between the plasma jet and the mainstream are convected along the upper side of the airfoil and transfer the momentum from the leading edge to the trailing edge.

Fig. 21 shows the evolution of swirling strength at different positions of the suction side of the airfoil. The calculation points are collected at a y position that corresponds to the maximum RMS velocity. Before actuation, the swirling strength is oscillating, and the average values are relatively low at different locations of the upper side of the airfoil. With the plasma actuator, the swirling strength is increased rapidly which is resulted from the small-size vortices and is still fluctuating. Meanwhile, the difference between swirling strengths without and with control is reduced at x^* = 0.3.

Indeed, some researchers obtained the dynamic process of flow separation control over an airfoil using a plasma actuator by wind tunnel experiments[50] and numerical simulation.[49] However, the flow structures in the vicinity of the surface of an airfoil have rarely been described due to the spatial resolution of PIV or huge computational resources and time. In this study, the detailed information near the wall is obtained by taking some measures to deal with surface reflections. Discrete rolling vortices which are moving along the surface of the airfoil are found, as shown in Fig. 18(b). Then these vortical structures are investigated in the power spectrum.

Fig. 22 shows power spectra of the vertical fluctuating velocity from x^* = 0.0013 to 0.3. The calculation points are obtained at a y position that corresponds to the maximum RMS speed. It is noteworthy that the first point which is located at x^* = 0.0013 is the starting point for shedding vortices. It is obvious that there is a distinct fundamental frequency of f_0 = 24 Hz in the first spectrum because of the issuing of rolling-up vortices close to the wall, as presented in Fig. 22(a). It is noteworthy that there exists a disparity of the fundamental frequency between the shedding vortices under incoming flow and the rolling-up vortices in quiescent air. It seems that the formation mechanisms are different. Under incoming flow, discrete rolling-up vortices are induced at the leading edge of the airfoil due to the interaction between the incoming flow and the induced airflow by the plasma actuator. Without incoming flow, roll-up vortices could be generated due to the instability of the shear layer. However, the mechanism of causing this disparity cannot be comprehensively elucidated by the present investigation and needs an in-depth study by further experiments. Then the shedding vortices start to grow, and a sub harmonic of the dominant frequency of 12 Hz appears at x^* = 0.1, as shown in Fig. 22(b). It indicates that the shedding vortices could be merged. Further downstream, there are multi-peak values which are not very conspicuous in the spectrum, as depicted in Fig. 22(c)–(d).

Based on the dominant frequency f_0 of 24 Hz, the cycle time was determined. Fig. 23 presents the development process of shedding vortices in one cycle by the swirling strength. Initially, the strength of a vortex which is at the leading edge of the airfoil is enhanced, as shown in Fig. 23(a). Then, this vortex is stretched longer because of the velocity gradient in the normal direction, and the swirling strength of the extended region at the leading edge of the airfoil is decreased, as depicted in Fig. 23(b). After that, a new vortex is issuing from the stretched region and moving along the suction side of the airfoil, as shown in Fig. 23(c). A train of discrete vortices travel into the trailing edge of the airfoil and transfer momentum to the separated region. Meanwhile, some vortical structures start to become less organized at x^* = 0.1, which means that these vortices could undergo a coalescence process, as presented in Fig. 23(d). The shear layer at the leading edge of the airfoil is extended again and accompanied by a reduction of the swirling strength, as shown in Fig. 23(e). At the following moment, a new vortex which is resulted from the extended region is shedding, as shown in Fig. 23(f).

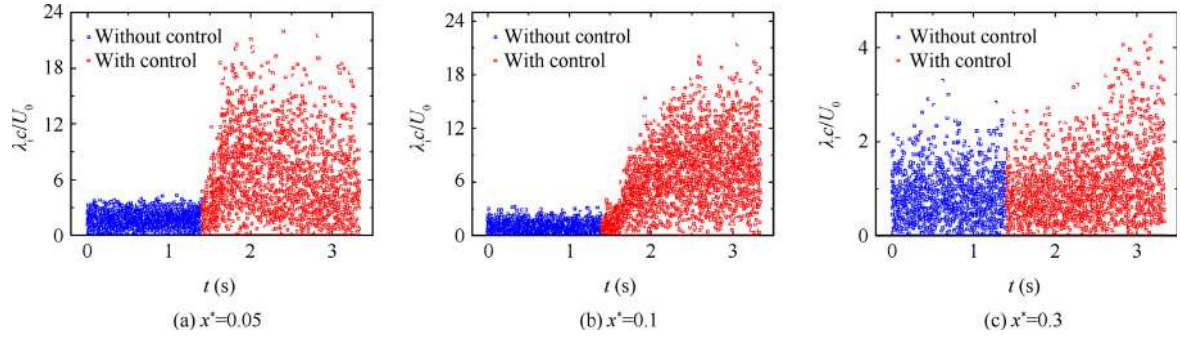

Fig. 21 Development process of swirling strength.

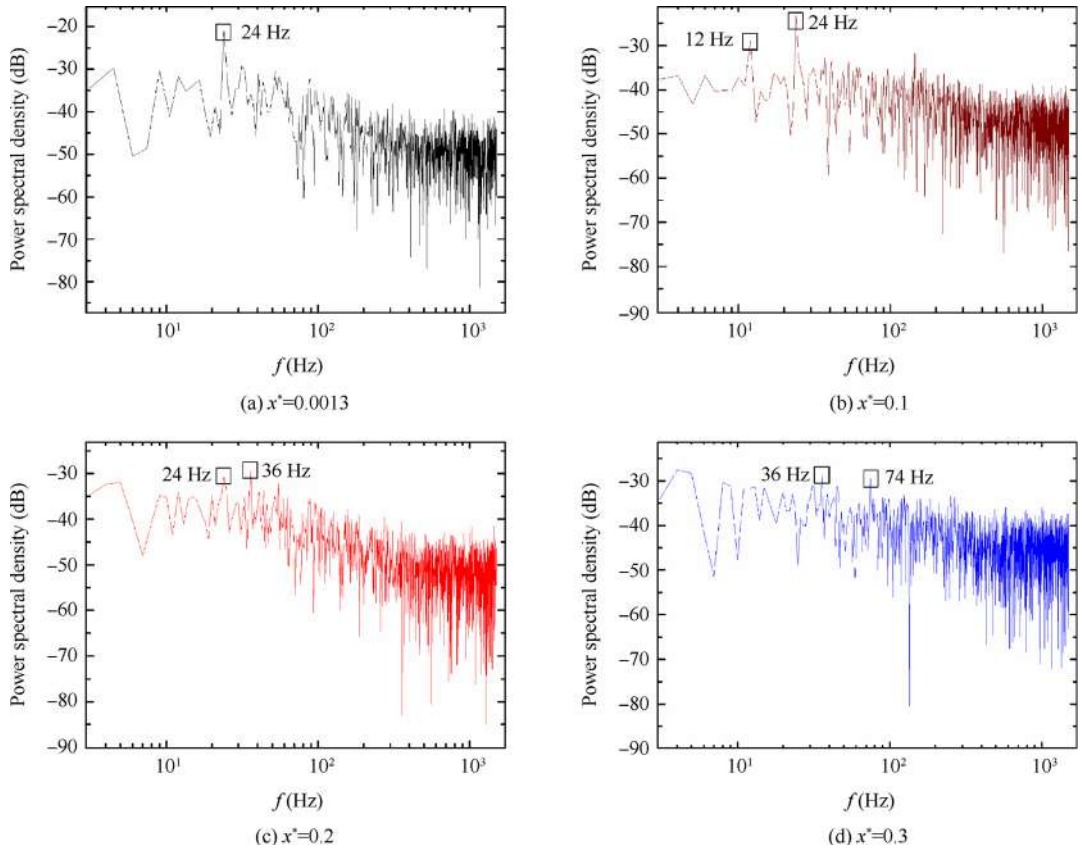

Fig. 22 Power spectra of vertical fluctuating velocity at different locations of upper side of airfoil with control.

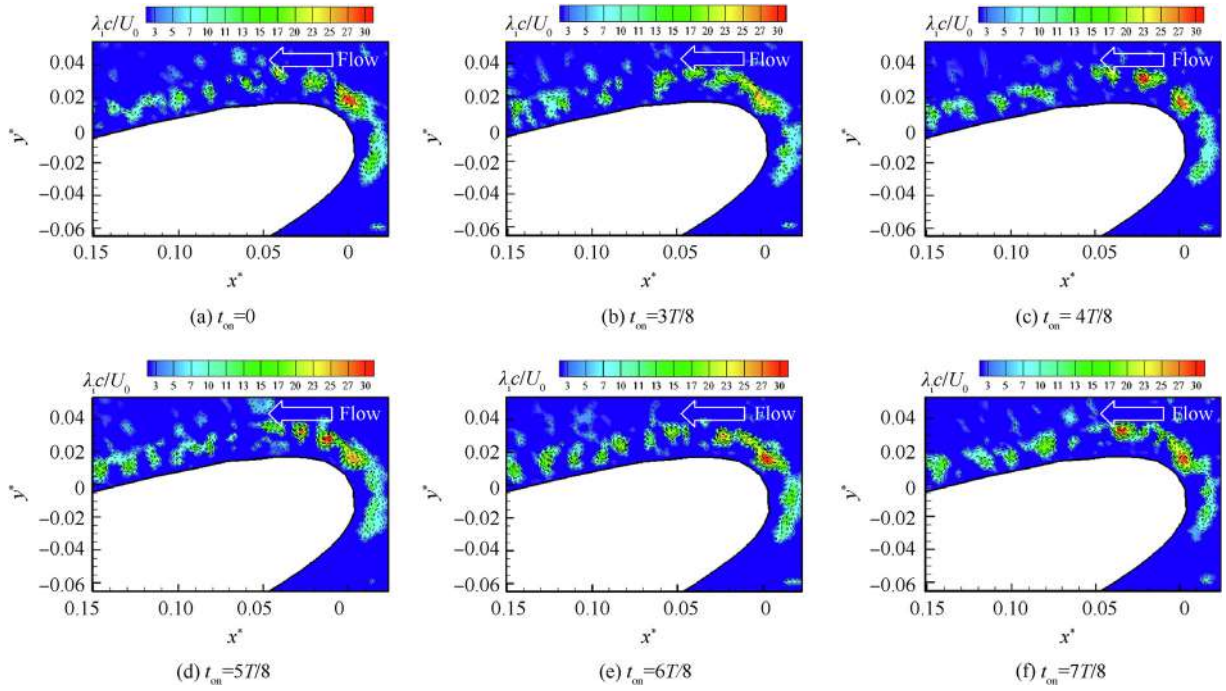

Fig. 23 Evolutions of discrete vortices on the upper side of airfoil in one cycle.

4. Conclusions

An experimental investigation of leading-edge flow separation control over a supercritical airfoil was carried out using a symmetrical DBD plasma actuator by a high-speed PIV system. This investigation was focused on the dynamic process of the interaction between the induced flow by the plasma actuator and the freestream. It was an attempt to deepen the understanding of the flow control mechanism of a DBD plasma actuator driven by an AC steady-mode excitation and mounted on the suction side of the airfoil near the leading edge.

Initially, a characterization of the symmetrical plasma actuator in quiescent air was performed. Results indicated that the symmetrical plasma actuator could generate a bi-directional jet which could have two types of jet, namely laminar jet and turbulent jet. This plasma jet could be affected by the voltage amplitude. When the voltage amplitude was low, the plasma jet was a laminar jet. The plasma jet became a turbulent jet which contained some coherent structures, such as roll-up vortices and secondary vortices, as the voltage amplitude was increased. These vortical structures were related to a dominant frequency of $f_0 = 39$ Hz and could promote the entrainment effect of higher momentum towards boundary layer flow through rolling and moving.

In addition, the based flow around the airfoil arranged at a high angle of attack ($\alpha = 18°$) was investigated in a low-speed wind tunnel. The velocity of incoming flow was 3 m/s. Results suggested that the vortices were shedding from the separated shear layer and linked to the fundamental frequency of $f_0 = 32$ Hz which was consistent with the finding of Yarusevych's investigations that the dominant frequency could be influenced by the Reynolds number.[58] These vortices grew and transferred the momentum from the incoming flow towards the suction side of the airfoil. Unfortunately, these vortices were not strong enough to suppress the separation by mixing.

Then, the controlled flow above the upper side of the airfoil was analyzed using time-averaged and time-resolved PIV measurements. The steady plasma actuation suppressed the separated flow around the airfoil which could be confirmed by the time-averaged velocity field. However, the flow could not be completely attached to the airfoil surface. What's more, results of the transient flow field highlighted that the development process of the interaction between the plasma jet and the freestream could be divided into three stages. At the beginning, the strength of shedding vortices was enhanced by the plasma actuator which acted as a catalyzer. After that, these vortical structures drew the separated flow above the upper side of the airfoil toward the airfoil surface, reducing the separated region around the airfoil. Finally, a series of discrete vortices in the vicinity of the airfoil surface was produced by the interaction between the induced flow by the plasma actuator and the incoming flow. These vortices could be responsible for the minor separation region near the wall, and transferred momentum to the separated region by travelling along the suction side of the airfoil, and were related to the dominant frequency of $f_0 = 24$ Hz.

Thanks to reducing the surface reflections and improving the spatial resolution, the vortical structures near the airfoil surface could be found. Here, this investigation opened a new insight concerning flow separation control over an airfoil by using a DBD plasma actuator with the steady mode. Further studies have to be carried out for figuring out the disparity of the fundamental frequency between the rolling-up vortices in still air and the shedding vortices under incoming flow. Meanwhile, a detailed investigation could be performed for understanding the relationship between the fundamental frequency of discrete rolling vortices and a number of parameters, such as voltage amplitude, actuation frequency, and the speed of freestream.

Acknowledgements

The authors are grateful to anonymous reviewers for their critical and constructive reviews of the manuscript. This study was supported by the Equipment Investigation in Advance of China (No. 51313010204).

References

1. Nickerson JD. A study of vortex generators at low Reynolds numbers. Reston: AIAA; 1986. Report No.: AIAA-1986-0155.
2. Seshagiri A, Cooper E, Traub LW. Effects of vortex generators on an airfoil at low Reynolds numbers. *J Aircraft* 2009;**46**(1):116–22.
3. Liebeck RH. Design of subsonic airfoils for high lift. *J Aircraft* 1978;**15**(9):547–61.
4. Wang JJ, Li YC, Choi KS. Gurney flap-lift enhancement, mechanisms and applications. *Prog Aerosp Sci* 2008;**44**:22–47.
5. Genc MS, Kaynak Ü. Yapici H. Performance of transition model for predicting low *Re* aerofoil flows without/with single and simultaneous blowing and suction. *Eur J Mech (B/Fluids)* 2011;**30**(2):218–35.
6. Atik H, Kim CY, Vandommelen LL, Walker JDA. Boundary-layer separation control on a thin airfoil using local suction. *J Fluid Mech* 2005;**535**:415–43.
7. Duvigneau R, Hay A, Visonneau M. Optimal location of a synthetic jet on an airfoil for stall control. *J Fluids Eng-Trans ASME* 2007;**129**(7):825–33.
8. Wang L, Luo ZB, Xia ZX. Energy efficiency and performance characteristics of plasma synthetic jet. *Acta Phys Sin* 2013;**62**(12):1–10 [Chinese].
9. Corke TC, Post ML, Orlov DM. Single dielectric barrier discharge plasma enhanced aerodynamics: Physics, modeling and applications. *Exp Fluids* 2009;**46**(1):1–26.
10. Li YH, Wu Y, Li J. Review of the investigation on plasma flow control in China. *Int J Flow Control* 2012;**4**(1):1–18.
11. Wang JJ, Choi KS, Feng LH, Jukes TN, Whalley RD. Recent developments in DBD plasma flow control. *Prog Aerosp Sci* 2013;**5**:1–27.
12. Wu Y, Li YH, Jia M. Experimental investigation into characteristics of plasma aerodynamic actuation generated by dielectric barrier discharge. *Chin J Aeronaut* 2010;**23**(1):39–45.
13. Che XK, Shao T, Nie WS, Yan P. Numerical simulation on a nanosecond-pulse surface dielectric barrier discharge actuator in near space. *J Phys D: Appl Phys* 2012;**45**(14):1–14.
14. Nie CQ, Li G, Zhu JQ. Investigation of dielectric barrier discharge plasma flow control. *Sci China Tech Sci* 2008;**51**(7):1064–72.
15. Zhang PF, Liu AB, Wang JJ. Flow structures in flat plate boundary layer induced by pulsed plasma actuator. *Sci China Tech Sci* 2010;**53**(10):2772–82.
16. Meng XS, Guo ZX, Luo SJ, Liu F. Control of asymmetric vortices over a slender conical forebody using plasma actuator. *Acta Aeronaut Astronaut Sin* 2010;**31**(3):500–5 [Chinese].
17. Liang H, Li YH, Song HM, Jia M, Wu Y. PIV investigation on flow induced by plasma aerodynamic actuation. *J Exp Fluid Mech* 2011;**25**(4):22–5 [Chinese].

18. Du H, Shi ZW, Geng X. Experimental study of directional-lateral aerodynamic moment control of micro air vehicle by plasma actuator. *Acta Aeronaut Astronaut Sin* 2012;**33**(10):1781–90 [Chinese].
19. Li Y, Zhang X, Huang X. The use of plasma actuators for bluff body broadband noise control. *Exp Fluids* 2010;**49**(2):367–77.
20. Inasawa A, Ninomiya C, Asai M. Suppression of tonal trailing-edge noise from an airfoil using a plasma actuator. *AIAA J* 2013;**51**(7):1695–702.
21. Jong AD, Bijl H. Corner-type plasma actuators for cavity flow-induced noise control. *AIAA J* 2014;**52**(1):33–42.
22. Feng LH, Jukes TN, Choi KS. Flow control over a NACA 0012 airfoil using dielectric barrier discharge plasma actuator with a Gurney flap. *Exp Fluids* 2012;**52**(6):1533–46.
23. Feng LH, Choi KS, Wang JJ. Flow control over an airfoil using virtual Gurney flaps. *J Fluid Mech* 2015;**767**:595–626.
24. Liang H, Wu Y, Li J. Test of high lift system flow control by plasma aerodynamic actuation. *Acta Aeronaut Astronaut Sin* 2016;**37**(8):2603–13 [Chinese].
25. Zhao GY, Li YH, Liang H. Flow separation control on swept wing with nanosecond pulse driven DBD plasma actuators. *Chin J Aeronaut* 2015;**28**(2):368–76.
26. Grundmann S, Tropea C. Experimental transition delay using glow-discharge plasma actuators. *Exp Fluids* 2007;**42**(4):653–7.
27. Kurz A, Goldin N, King C, Tropea C, Grundmann S. Hybrid transition control approach for plasma actuators. *Exp Fluids* 2013;**54**(11):1–4.
28. Lu JC, Shi ZW, Du H. Experimental study of controlling flat transition using surface dielectric barrier discharge actuator. *Acta Aeronaut Astronaut Sin* 2016;**37**(4):1166–73 [Chinese].
29. Jukes TN, Choi KS. Flow control around a circular cylinder using pulsed dielectric barrier discharge surface plasma. *Phys Fluids* 2009;21:084103.
30. Li WF, Cai JS, Hao JN, Liu QH. Flow control on a circular cylinder using multi-bipolar plasma actuator. *J Exp Fluid Mech* 2013;**27**(3):17–22 [Chinese].
31. Wu Y, Li YH. Progress and outlook of plasma flow control. *Acta Aeronaut Astronaut Sin* 2015;**36**(2):381–405 [Chinese].
32. Li YH, Wu Y, Zhou M. Control of the corner separation in a compressor cascade by steady and unsteady plasma aerodynamic actuation. *Exp Fluids* 2010;**48**(6):1015–23.
33. Shi ZW, Fan BG. Experimental study on flow control characteristics of different plasma actuator. *Acta Aeronaut Astronaut Sin* 2011;**32**(9):1583–9 [Chinese].
34. Han MH, Li J, Niu ZG. Aerodynamic performance enhancement of a flying wing using nanosecond pulsed DBD plasma actuator. *Chin J Aeronaut* 2015;**28**(2):377–84.
35. Wu Z, Wong CW, Wang L, Lu Z, Zhu Y, Zhou Y. A rapidly settled closed-loop control for airfoil aerodynamics based on plasma actuation. *Exp Fluids* 2015;**56**(8):1–15.
36. Che XK, Nie WS, Zhou PH, He HB, Tian XH, Zhou SY. Study on continuous vortices induced by sub-microsecond pulsed surface dielectric barrier discharge plasma. *Acta Phys Sin* 2013;**62**(22):224702 [Chinese].
37. Zhang X, Huang Y, Wang XN, Wang WB, Tang K, Li HX. Flow control on a supercritical wing using dielectric barrier discharge plasma actuator. *Acta Aeronaut Astronaut Sin* 2016;**37**(6):1733–42 [Chinese].
38. Sun Q, Cheng BQ, Li YH. Computational and experimental analysis of Mach 2 air flow over a blunt body with plasma aerodynamic actuation. *Sci China Tech Sci* 2013;**56**(11):795–802.
39. Little J, Nishihara M, Adamovich I. High-lift airfoil trailing edge separation control using a single dielectric barrier discharge plasma actuator. *Exp Fluids* 2010;**48**(3):521–37.
40. Kelley CL, Bowles PO, Cooney J, He C, Corke TC, Osborne BA, et al. Leading-edge separation control using alternating-current and nanosecond-pulse plasma actuators. *AIAA J* 2014;**52**(9):1871–84.
41. Sosa R, Artana G, Benard N, Moreau E. Mean lift generation on cylinders induced with plasma actuators. *Exp Fluids* 2011;**51**(3):853–60.
42. Patel MP, Sowle ZH, Corke TC. Autonomous sensing and control of wing stall using a smart plasma slat. *J Aircraft* 2007;**44**(2):516–27.
43. Chen ZL, Hao LZ, Zhang BQ. A model for NanoSecond pulsed Dielectric Barrier Discharge (NSDBD) actuator and its investigation on the mechanisms of separation control over an airfoil. *Sci China Tech Sci* 2013;**56**(5):1055–65.
44. Orlov DF, Apker T, He C, Othman H, Corke T. Modeling and experiment of leading edge separation control using SDBD plasma actuators. Reston: AIAA; 2007. Report No.: AIAA-2007-0877.
45. Roupassov D, Nikipelov A, Nudnova M. Flow separation control by plasma actuator with nanosecond pulsed-periodic discharge. *AIAA J* 2009;**47**(1):168–85.
46. Post ML, Corke TC. Separation control on high angle of attack airfoil using plasma actuator. *AIAA J* 2004;**42**(11):2177–84.
47. Bouremel Y, Li JM, Zhao ZJ, Debiasi M. Effects of AC Dielectric Barrier Discharge plasma actuator location on flow separation and airfoil performance. *Proceedings of 2013 Asian-Pacific conference on aerospace technology and science*; 2013 May 23-26; Taiwan, China. 2013.
48. Balcon N, Benard N, Lagmich Y, Boeuf JP, Touchard G, Moreau E. Positive and negative sawtooth signals applied to a DBD plasma actuator—Influence on the electric wind. *J Electrost* 2009;**67**(2):140–5.
49. Sato M, Nonomura T, Okada K, Asada K, Aono H, Yakeno A, et al. Mechanisms for laminar separated-flow control using dielectric-barrier-discharge plasma actuator at low Reynolds number. *Phys Fluids* 2015;27:117101.
50. Benard N, Moreau E. On the vortex dynamic of airflow reattachment forced by a single non-thermal plasma discharge actuator. *Flow Turbul Combust* 2011;**87**:1–37.
51. Greenblatt D, Schneider T, Schule CY. Mechanism of flow separation control using plasma actuation. Phys Fluids 2012;24:077102.
52. Sekimoto S, Nonomura T, Fujii K. Burst-mode frequency effects of dielectric barrier discharge plasma actuator for separation control. *AIAA J* 2017;**55**(4):1385–92.
53. Zhang X, Huang Y, Wang WB. Unmanned air vehicle flow separation control using dielectric barrier dis-charge plasma at high wind speed. *Sci China-Phys Mech Astron* 2014;**57**(6):1160–8.
54. Zhang X, Li HX, Huang Y. Wing flow separation control using asymmetrical and symmetrical plasma actuator. *J Aircraft* 2017;**54**(1):301–9.
55. Dovgal AV, Kozlov VV, Michalke A. Laminar boundary layer separation: instability and associated phenomena. *Prog Aerosp Sci* 1994;**30**:61–94.
56. Zhou J, Adrian RJ, Balachandar S, Kendall TM. Mechanisms for generating coherent packets of hairpin vortices in channel flow. *J Fluid Mech* 1999;**387**:353–96.
57. Zhang C, Pan C, Wang JJ. Evolution of vortex structure in boundary layer transition induced by roughness elements. *Exp Fluids* 2011;**51**:1343–52.
58. Yarusevych S, Sullivan P, Kawall JG. On vortex shedding from an airfoil in low-Reynolds-number flows. *J Fluid Mech* 2009;**632**:245–71.
59. Lang M, Rist U, Wagner S. Investigations on controlled transition development in laminar separation bubble by means of LDA and PIV. *Exp Fluids* 2004;**36**(1):43–52.
60. Roth JR. Aerodynamic flow acceleration using paraelectric and peristaltic electrohydrodynamic effects of a one atmosphere uniform glow discharge plasma. *Phys Plasmas* 2013;**10**(5):2117.